CFD SIMULATIONS OF THE FLOW MIXING IN THE LOWER PLENUM OF PWR'S

G. Pochet, M. Haedens, C.R. Schneidesch, D. Léonard

GDF SUEZ - Tractebel Engineering
7 Ave. Ariane, 1200 Brussels, Belgium
Tel: +32 2 773 8386, Fax +32 2 773 8900

Abstract

To ensure an accurate simulation of the interactions between physical phenomena arising during complex accidents, multi-physics approaches are developed at Tractebel Engineering (TE) by coupling best estimate codes. In asymmetric conditions, one of the most important issues is the evaluation of the core inlet temperature distribution, which is strongly determined by the flow mixing in the lower plenum. More accurate modeling of the mixing can be obtained from CFD. Three experimental tests conducted during the FLOMIX-R project (Rohde, 2005 ; Toppila, 2004) are simulated. Qualitative code validation is made by varying the time step, turbulence model and spatial mesh resolution. The comparison shows that the main phenomena observed during the experiments are reproduced in the simulations. In the second step a CFD model of the Tihange 3 pressure vessel is developed. Several simulations are performed to investigate the effect of different asymmetric conditions on the flow mixing in the lower plenum. The simulation results point out the mixing dependency on the considered loop and on its temperature. The implementation of the CFD core inlet distributions in the coupled code package at TE has the potential to yield a more realistic evaluation of the safety margins in the Final Safety Analysis Report.

1. INTRODUCTION

Flow mixing in PWR's is an important phenomenon that plays a significant role in the course of particular accidents. More precisely, accidents leading to an asymmetric temperature distribution between the loops are of primary concern (steam and feedwater line breaks). During such accidents, the affected loop cold leg temperature is different compared to the other cold legs. Flow mixing in these conditions is a key parameter because it will determine the temperature distribution at the core inlet. Moreover, since the flow temperature strongly influences the neutronic response of the fuel assemblies, its assessment requires particular attention for the evaluation of the departure from nucleate boiling ratio (DNBR).
Because of the strong interaction between thermal-hydraulics and neutronics in these conditions, current analyses of these accidents are performed by coupling codes and solving together system thermal-hydraulics, core thermal-hydraulics and core neutronics. The aim of the present work lies at the interface between thermal-hydraulics and neutronics. Indeed, the purpose of the study is to improve the coupled methodology developed at TE for assessing SLB (steam line break) and FWLB (feedwater line break) accidents, by providing a more accurate modeling of the flow mixing in the lower plenum of the vessel.

The first step of the work focuses on a benchmark of the ANSYS CFX code. For this purpose the experimental results of the steady-state mixing experiments conducted in the FLOMIX-R project (Rohde, 2005 ; Toppila, 2004) are used. The purpose of this step is to validate the code for single phase turbulent mixing in complex 3D structures. Indeed, this validation process is necessary to allow the use of the CFD method for the flow mixing analysis in the Belgian PWR's. An extensive validation work on the applicability of CFD methods for simulating the ROCOM mixing experiments has already been performed and can be found in the literature (Höhne, 2007 ; Kliem, 2009 ; Prasser, 2003 ; Rohde, 2005 ; Rhode, 2007 ; Rhode, 2009 ; Toppila, 2004). The most important conclusions of these previous studies

concerning grid and time step size, turbulence models, boundary conditions and numerical schemes are used to justify the choices made for the present simulations. The CFD model of the ROCOM pressure vessel is built by taking into account the geometrical details of the internal structures. Steady-state simulations are performed with several spatial mesh resolutions, and particular importance is given to the height of the wall-adjacent cells. Due to limited computer resources, fully mesh-independent solutions can not be reached and the optimum mesh is chosen for the transient simulations. Three different experiments are simulated, three time step sizes are considered and two turbulence models are tested. The comparison of the simulation results with the experimental data shows that the code is able to predict the mixing behavior observed in the experiments. However, limited statistical analyses are performed to assess the results quantitatively, due to the lack of numerical experimental data.

The second step of the work consists in developing a CFD model of the Tihange 3 reactor pressure vessel, and to quantify the flow mixing in the lower plenum. The objectives of the CFD simulations are to assess two main parameters that play a significant role in the current coupled methodology at TE for analyzing asymmetric accidents: the loop mixing coefficients and the flow distribution at the core inlet. A more accurate description of these objectives is provided in the next section when presenting the TE coupled methodology. Since the internal structures are expected to strongly influence the flow mixing, all penetrations and their support plates are represented in detail in the lower plenum. Due to time constraints, only one mesh is generated. Mesh refinement is applied in regions where high flow gradients are expected, and the height of the wall-adjacent cells is specified to yield the recommended range of y^+ values. Steady-state simulations are performed, and three different cases are studied: one case to simulate the normal operation of the reactor during which all three loops are at the same temperature, and two additional cases to investigate the influence of the higher affected loop cold leg temperature on the flow mixing. The results demonstrate the different mixing behavior of the loops due to the asymmetry of the pressure vessel, and show the local influence of the temperature on the flow mixing.

The structure of this paper is the following. In section 2 the current coupled methodology applied at TE for asymmetric accident analyses is presented, in order to justify and describe the objectives of the present study. In section 3 the CFD model of the ROCOM pressure vessel is described, and the comparison of the simulation results with the experimental data is performed to validate the CFD code. Section 4 is dedicated to the CFD model of the Tihange 3 pressure vessel, and assessments of the flow mixing are performed for different conditions and discussed with the mixing assumptions implemented in the current TE coupled methodology. Finally the conclusions are drawn in Section 5.

2. COUPLED METHODOLOGY AT TE AND OBJECTIVES OF THE STUDY

The nuclear reactor accident analyses using best estimate codes provide a better understanding and more accurate modeling of the key physical phenomena. However, these key physical phenomena might be of different nature (neutronics/thermal-hydraulics) and they can strongly interact during complex accidents to have a definite impact on the transient behavior. It is therefore necessary to ensure an accurate simulation of these interactions. Such accuracy can be obtained by means of multi-physics approaches which consist of taking simultaneously into account all these different phenomena.

At TE, multi-physics approaches are developed by coupling different best estimate codes. Figure 1 illustrates the data exchange process when coupling the RELAP5 system thermal-hydraulics code to the PANTHER[1] neutronics code. This approach is used for simulating accidents leading to an asymmetric temperature distribution between the loops, like for steam and feedwater line break accidents. To account for the different loop flow conditions, the model of the vessel in RELAP5 is split in three sectors, one sector corresponding to each loop (Tihange 3 unit, three loops PWR). On the thermal-hydraulics side, the flow mixing is modeled by imposing mixing coefficients at the junctions between the lower plenum and the core inlet of each sector. On the neutronics side, the flow mixing is modeled in a dedicated interface

[1] PANTHER is a computer program developed by British Energy Generation and distributed by the ANSWERS Service (Serco Assurance, Winfrith UK).

that combines the cold legs enthalpy and mass flow rate calculated by RELAP5, and generates the core inlet distribution to be imposed as boundary condition for the PANTHER core model. The current flow mixing assumptions rely on conservative distributions derived from a limited number of experimental results. Moreover, these experimental results were not collected in the pressure vessel of interest. Therefore, more accurate reproduction of the flow mixing can be obtained from CFD simulations that allow combining local geometrical effects to flow turbulence. One branch of the improvements at TE of the coupling between neutronics and thermal-hydraulics focuses on the implementation of core inlet distributions obtained from CFD results. The improved coupled code package will yield a more realistic evaluation of the safety margins in the Final Safety Analysis Report.

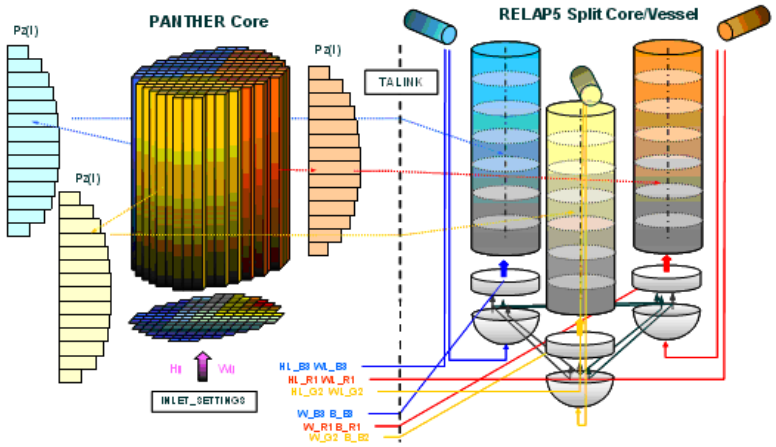

Figure 1: Data exchange process between the RELAP5 and PANTHER codes in the coupled methodology

3. BENCHMARK OF THE ANSYS CFX CODE

Figure 2 (left) represents the CFD model of the ROCOM pressure vessel. The model has been built by following the recommendations found in literature (Rohde, 2007). The flow in the core has been modeled by a free flow field, since this simplification is not expected to have a great influence on the flow mixing in the lower plenum. On the other hand, since the internal structures significantly affect the flow mixing, the complex geometry of the sieve drum has been modeled in detail. Furthermore, the outlet nozzles have been represented to take into account the asymmetrical outflow effects at the cold leg nozzles. For generating the meshes, the domain has been divided in two parts: the upper part of the vessel comprising the cold legs and the downcomer, and the lower part of the vessel composed of the lower plenum, the core plate, and the core region. From these two parts different combinations of meshes were made (see Table 1). All the generated meshes are unstructured hybrid meshes composed mainly of tetrahedral elements, but containing also prisms and pyramids. Using hexahedral meshing particularly for the downcomer region is foreseen for future sensitivity studies. When looking at Table 1, in a first step the same spatial mesh resolution was kept for the upper part of the vessel, and successive mesh refinement was applied for the lower part (sequence of meshes 1-2-3-5). In the second step the same spatial mesh resolution was kept for the lower part, and mesh refinement was applied for the upper part (sequence of meshes 3-4). Mesh refinement has been performed in regions where higher flow gradients are expected: inlet and outlet nozzles connection with the pressure vessel, downcomer extension, sieve drum and core plate holes. To capture the boundary layer effects, the height of the wall-adjacent cells has been specified to yield the required range of y^+ values. The resulting y^+ values in the downcomer are below 200 for meshes 4 and 5. Figure 2 (middle and right) shows the visualization for one of the generated mesh (Mesh 5).

3.1 Steady-state simulations

Preliminary steady-state simulations were performed to determine the optimum mesh for the transient simulations. For the inlet the same volume flow rate of 185 m³/h was imposed uniformly in each cold leg, corresponding to the conditions of the ROCOM-STAT-01 experiment. For the outlet a pressure boundary condition was imposed. Following the conclusions found in literature (Rohde, 2007), as the results of the steady-state mixing simulations are not very sensitive to the turbulence model, the $k-\omega$ SST turbulence model with automatic wall functions was used for all steady-state simulations. Since higher order scheme should be used, the high resolution scheme of ANSYS CFX was used for the spatial discretization. Due to limited computer resources, the double precision was switched off.

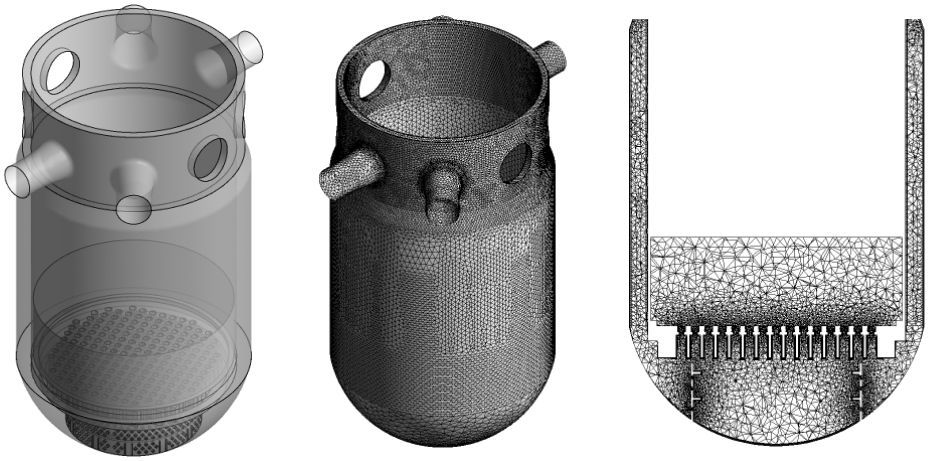

Figure 2: CFD model of the ROCOM pressure vessel (left) and visualization for one of the generated mesh (middle and right)

Table 1: Number of volume elements for the different meshes

Part of the vessel	Elements	Mesh 1	Mesh 2	Mesh 3	Mesh 4	Mesh 5
Upper part	598246					
	1046740					
Lower part	666050					
	844172					
	1302528					
	1613230					

Figure 3 shows the results obtained with the different meshes for the vertical velocity profile in the lower downcomer. The figure also shows the experimental results for two realizations of the ROCOM-STAT-01 mixing experiment along with their confidence interval (Rohde, 2005 ; Toppila, 2004). It can be seen that the calculation results show qualitatively good agreement with the experimental data: minima and maxima of the velocity are observed at the same locations. However, the calculated minima and maxima are respectively smaller and higher than in the experiments for all calculations. Also there is a shift to the left of the calculated velocity profile below loop 3 and 4 compared to the calculations. From the results it can be concluded that the refinement of the mesh does not affect significantly the velocity profile in the downcomer. For each simulation, the number of calculated velocities located in the confidence interval of experiment D10 (curve in red) has been determined. Among the 64 calculated velocities, the greatest number is obtained for Mesh 5 with 41 points located in the confidence interval. For this reason, the transient calculations have been performed on the optimum mesh 5.

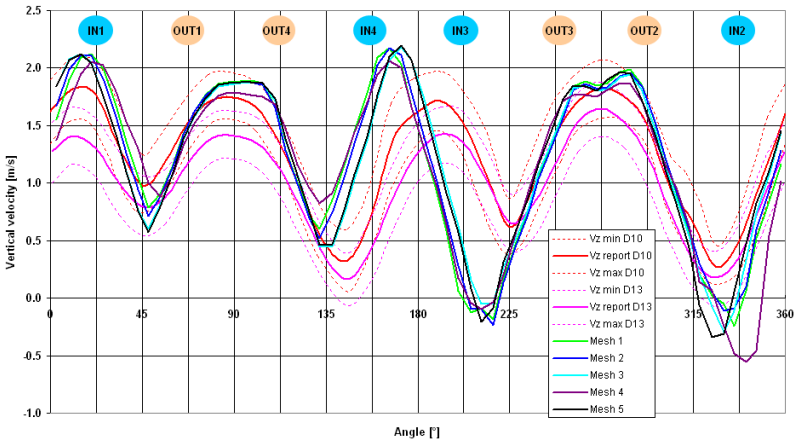

Figure 3: Vertical velocity profile in the downcomer

3.2 Transient simulations

Three different experiments have been simulated: ROCOM-STAT-01 (nominal flow rate in all loops), ROCOM-STAT-08 (10 % asymmetry between two loops, nominal total flow rate) and ROCOM-STAT-09 (20 % asymmetry between two loops, nominal total flow rate). A scalar variable simulating the tracer was imposed in one loop for 7 seconds. Three time step sizes were considered: 0.1, 0.05 and 0.02 s. Also two turbulence models were used: the $k-\omega$ SST turbulence model with automatic wall functions was used for the three experiments and the $k-\varepsilon$ model with scalable wall functions was used for experiment ROCOM-STAT-08.

Figure 4 gives the experimental (Toppila, 2004) and simulation results for the time evolution of the mixing scalar at both downcomer sensors, for the experiments with growing asymmetry. For the simulation results, each of the 64 measurement positions located along the middle radius of the downcomer sensors was used at each time step (0.05 s). It can be seen that the simulation results correspond quite well to the experiments. Indeed, in both the experiments and the calculations it is observed that the sector covered by the tracer in the downcomer increases with the loop flow rate, the right border being displaced towards the closest adjacent loop of the tracer injection. At the lower downcomer sensor, it is clearly seen in the experiments with loop asymmetry that the tracer splits and that the highest concentrations stay at the left border. Despite the concentrations are overestimated near to the right border, this effect is also visible in the calculations. The small line of tracer due to a recirculation area in the downcomer (Toppila, 2004) is predicted in the simulations, but only at the upper downcomer sensor, while at the lower sensor this small amount of tracer is back to the bulk. Finally, the small area with zero concentration at the tracer front for the lower sensor is also reproduced. This area is observed between azimuthal positions corresponding to the inlet and outlet nozzles of loop 1, and is due to the velocity profile in the lower downcomer. Indeed, at this azimuthal position the velocity reaches a minimum (see Figure 3). The influence of the time step on the results was found to be negligible. However, the $k-\omega$ SST turbulence model was found to give better results than the $k-\varepsilon$ model. Indeed, with the $k-\varepsilon$ model for experiment ROCOM-STAT-08 the zero concentration area at the tracer front in the lower downcomer is exaggerated.

Figure 5 shows the experimental (Toppila, 2004) and calculated plateau averaged mixing scalar at the core inlet for experiment ROCOM-STAT-01. As it can be seen from this figure the contours in the calculations have a different shape compared to the contours observed in the experiment. Indeed the contours are less closed in the calculation, which means that the highest spot of tracer is more spread in the calculation. The maximum value of the mixing scalar is 3 % lower in the calculation, but its location is close to the experimental results (1 assembly position next to the real location). When comparing both figures it can be seen that the calculation predicts higher values for the mixing scalar in the region near to

the closest adjacent loop of the tracer injection. This higher tracer concentration in this region was already observed in the downcomer (see Figure 4). It can also be seen that the calculation predicts lower values for the mixing scalar at the border of the tracer sector and that the sector covered by the tracer is smaller in the calculation. As for the tracer distribution at the downcomer sensors, no influence of the time step on the contours has been observed either.

Figure 6 shows the experimental (Toppila, 2004) and calculated plateau averaged mixing scalar at the core inlet for the experiment ROCOM-STAT-08. The agreement between the experiments and the calculation results is better than for the nominal flow rate case. Indeed, the shape of the contours is similar. The location of the calculated maximum is close to the experiment (1 assembly position next to the real location) and the calculated value is 1.8 % lower. However, the distribution of the errors is identical than for the nominal flow rate case: the tracer concentrations are higher near to the position corresponding to the closest adjacent loop of the tracer injection, and lower concentrations are found at the border of the tracer sector.

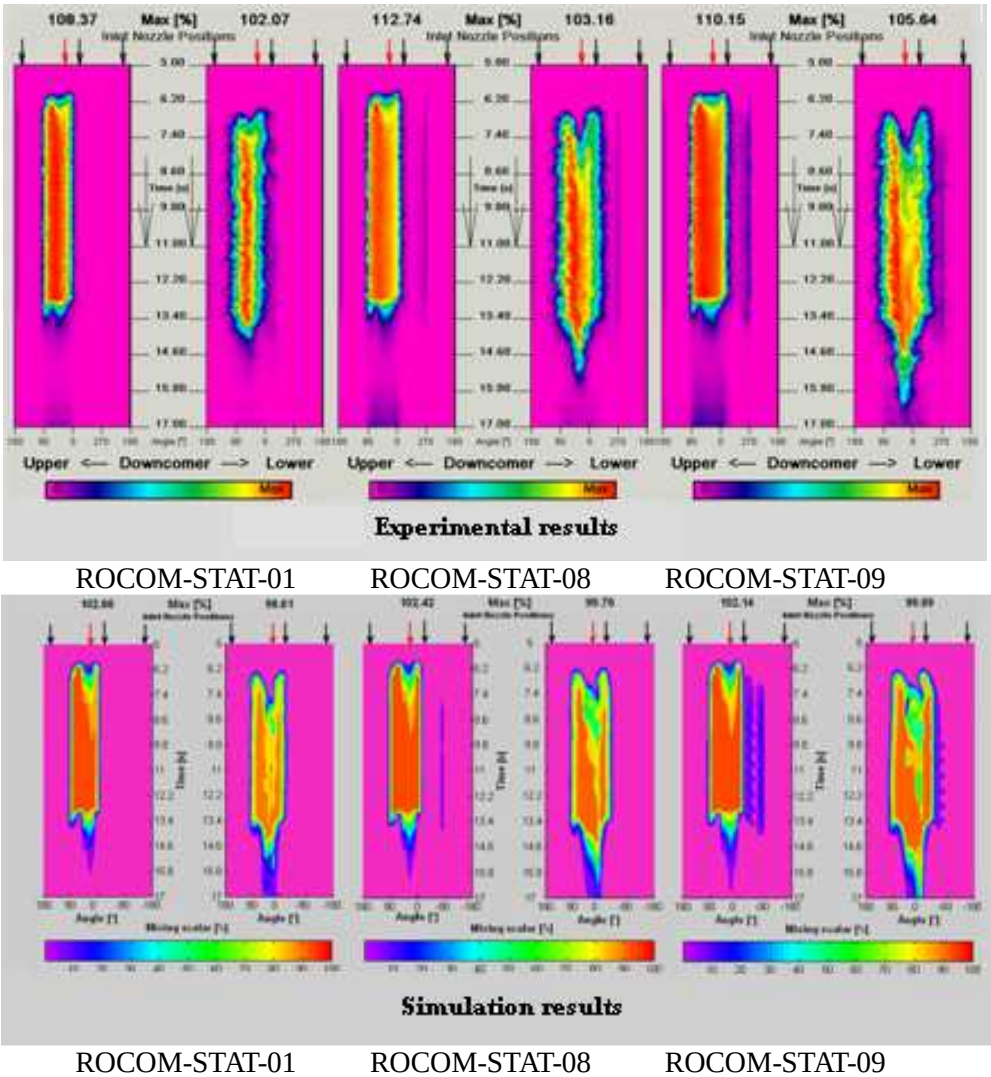

Figure 4: Time evolution of the mixing scalar at the downcomer sensors for the experiments with growing asymmetry (simulation results are shown for the k-ω SST turbulence model)

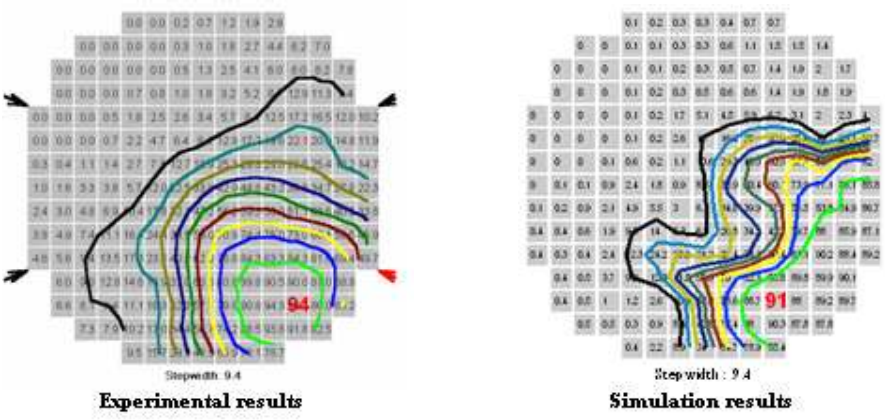

Figure 5: Plateau averaged mixing scalar at the core inlet sensor for experiment ROCOM-STAT-01

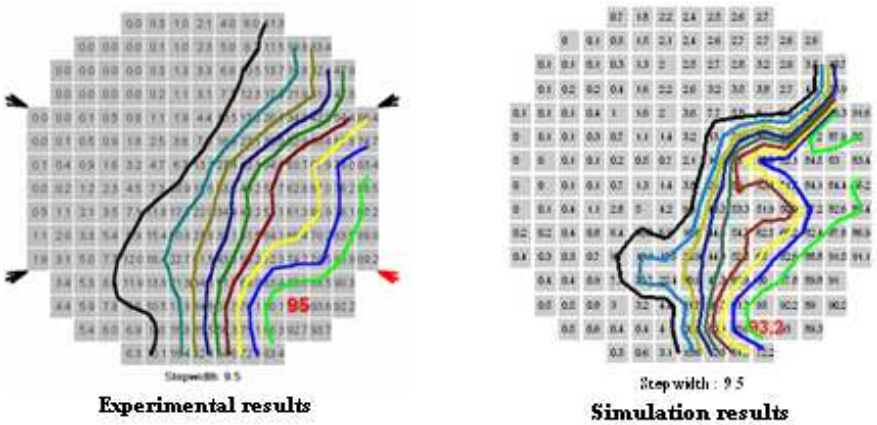

Figure 6 : Plateau averaged mixing scalar at the core inlet sensor for experiment ROCOM-STAT-08 (simulation results are shown for the k-ω SST turbulence model)

For the quantitative assessment of the results, the root mean square of the errors was calculated:

$$\mathrm{Error_i} = \mathrm{Calculated_i} - \mathrm{Measured_i} \tag{1}$$

$$Error_{RMS} = \sqrt{\frac{1}{n}\sum_{i=1}^{n} Error_i^2} \tag{2}$$

where i goes through all the measurement positions and n is the total number of measurement positions. Table 2 gives the calculated root mean square errors for the different calculations. As expected the RMS error is higher for experiment ROCOM-STAT-01 and lower for the experiments with loop asymmetry. The best agreement with the experimental results is obtained for experiment ROCOM-STAT-08. As for the tracer distribution at the downcomer sensors, the $k-\omega$ SST turbulence model gives better results than $k-\varepsilon$.

Future sensitivity studies are foreseen on hexahedral meshing, and particularly in the downcomer region. If feasible, some regions in the lower plenum should also be meshed with hexahedral elements. Indeed, the low mesh quality obtained in the lower plenum when using tetrahedral elements in this complex geometry is thought to be partly responsible for the disagreements observed at the core inlet. Using hexahedral elements is expected to decrease numerical diffusion and to give insight on these disagreements.

Table 2: RMS error for the different simulations

Experiment	RMS error [%]
ROCOM-STAT-01	18.0
ROCOM-STAT-08 ($k-\omega$ SST turbulence model)	9.1
ROCOM-STAT-08 ($k-\varepsilon$ turbulence model)	12.4
ROCOM-STAT-09	12.1

4. FLOW MIXING ASSESSMENT IN THE TIHANGE 3 RPV

Figure 7 represents the CFD model of the Tihange 3 pressure vessel. Since the work focuses on flow mixing in the lower plenum, the flow has been modeled from the inlet nozzles up to only 1/5 of the core height. The fuel assemblies have not been represented in detail, but instead the core free surface was extruded (section available for the flow in the core when omitting all fuel assemblies). This baffle shaped like volume modeling the flow in the core will be treated by the code as two different regions (see right side of Figure 7). The first part will be treated as a fluid region since it models the flow at the foot of the fuel assemblies, and there it might be assumed that the section available for the flow is the same as the core free surface. The second part which represents 1/5 of the active core region will be treated by the code as a porous region. This simplification is acceptable since the active core volume is dense in regular structures (157 fuel assemblies, each of them composed of a 17x17 fuel rods pattern). There are four thermal shields in the downcomer. The bottom instrumentation consists of 50 penetrations held by 3 support plates. The penetrations have not been modeled in detail, but instead they have been represented by one cylinder with constant section. There are four holders for the core barrel, and three of them are visible on Figure 7. At the core inlet plate, each fuel assembly inlet consists of four water holes. Each of the 50 bottom penetrations is centered on a fuel assembly, that is, in the middle of four water holes.

Given the complexity of the model, the domain was divided in four parts that were meshed separately: the downcomer, the lower plenum, the foot of the assemblies and the active core region. Due to time constraints, no mesh sensitivity has been performed but a single fine unstructured hybrid mesh was generated (tetrahedral, prismatic and pyramidal elements). Future sensitivity studies are foreseen on mesh resolution and on hexahedral meshing. Table 3 gives the number of elements for each part of the domain and for the total domain. To yield the required range of y^+ values, the height of the wall-adjacent cells was specified to 0.05 mm. Mesh refinement has been performed in regions near to the inlet nozzles connection with the pressure vessel, the outlet nozzles, the thermal shields, the bottom penetrations and their support plates, and the core plate water holes.

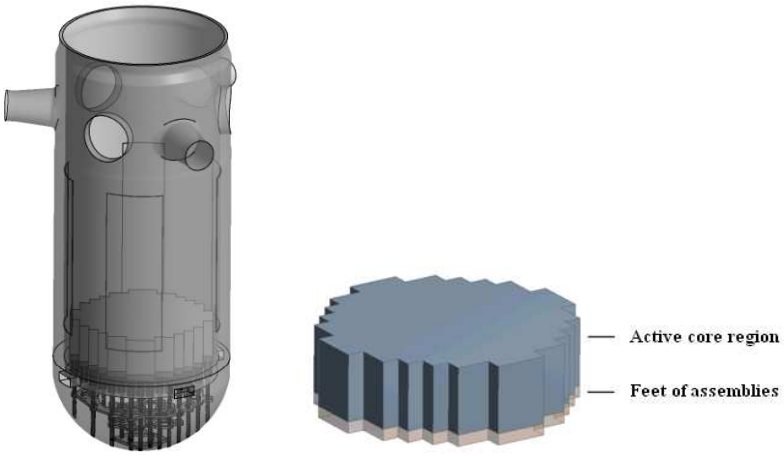

Figure 7: CFD model of the Tihange 3 pressure vessel (left) and core model (right)

Table 3: Number of mesh elements for each part of the domain and for the total domain

Part	Number of elements
Downcomer	2252145
Lower plenum	2108509
Assemblies foot	43018
Active core region	254764
Total model	4658436

For the inlet boundary condition, the loop volume flow rate to be considered amounts to 22380 m³/h. The inlet boundary condition was imposed by specifying the following developed velocity profile for each of the three inlets:

$$U(r) = U_{max}(1 - \frac{r}{R})^{\frac{1}{7}} \quad (3)$$

where U_{max} is the maximum velocity reached at the centre of the cold leg inlet, which has to be calculated to obtain the correct volume flow rate, R is the internal radius of the cold leg, and r is the radial position on the section of the cold leg inlet. A pressure boundary condition was imposed for the outlet. The $k-\omega$ SST turbulence model was used for all the simulations, since this model gave the best results for the ROCOM calculations. Three different cases were studied, depending on the temperature condition in each loop:

- Case 1 : T = 293.5°C for each loop
- Case 2 : T = 336.8°C for loop 2, T = 293.5°C for loops 1 and 3
- Case 3 T = 336.8°C for loop 3, T = 293.5°C for loops 1 and 2

The value of 293.5°C corresponds to the nominal temperature, while 336.8°C corresponds to the maximum temperature reached in the reference case for a FWLB calculated with the RELAP5 system code at TE. The aim of the second and third simulations is to analyse the influence of the temperature on the flow mixing.

4.2 Mixing coefficients

To quantify the mixing coefficients, a scalar tracer variable was defined for each loop. Since the mass flow of the tracer variables is conserved over the simulation domain, the mixing coefficients can be determined by the following equation:

$$Loop\ i\ mixing\ coefficient = \frac{\int_{A_{sector}} \rho v \phi_i \, dA}{\int_{A_{core}} \rho v \phi_i \, dA} \times 100 \quad (4)$$

where A_{sector} is the section of the core inlet sector associated to loop i, A_{core} is the total section at the core inlet, v is the vertical component of the velocity, and Φ_i is the scalar tracer variable associated to loop i. In order to be conservative, the core inlet sectors are defined in such a way that they maximize the mixing coefficients. Indeed, in safety analyses of asymmetric accidents, conservative assumptions have to be made concerning the flow mixing. Sectors have also been implemented in the downcomer, in order to distinguish the mixing in the downcomer from the mixing in the lower plenum. The application of equation (4) for calculating the mixing coefficients in the downcomer is straightforward. To determine the sectors configuration, a sector of 120° was defined. Starting from a position, the sector was successively rotated by 1° until 360° and the mixing coefficients were evaluated after each rotation. Table 4 gives the

mixing coefficient in the downcomer and at the core inlet for each loop resulting from this analysis. As it can be seen from the table, the mixing coefficients are not equivalent for the three loops. This is due to the asymmetry of the reactor pressure vessel. Indeed, the pressure vessel has three loops but four thermal shields and four holders for the core barrel are found, and the water holes in the core inlet plate do not present one third symmetry. Moreover, the position of the bottom penetrations as well as the geometry of the support plates is not symmetric around the vessel either. The different mixing behavior of the loops can be observed on Figure 8 which gives the tracer distribution at the core inlet for each loop. This analysis of the mixing coefficients demonstrates the conservatism used in the current coupled methodology. Indeed, the value considered for the core inlet mixing coefficient in the RELAP5 split vessel model amounts to 85 %. Therefore, it is expected to gain some margin limits in the safety studies if the mixing coefficients calculated by the CFD method are considered in the RELAP5 split vessel model.

Table 4 : Calculated mixing coefficient (case 1)

	Mixing coefficient [%]		
Region	**Loop 1**	**Loop 2**	**Loop 3**
Core inlet	53.4	68.1	59.5
Downcomer	68.4	91.2	92

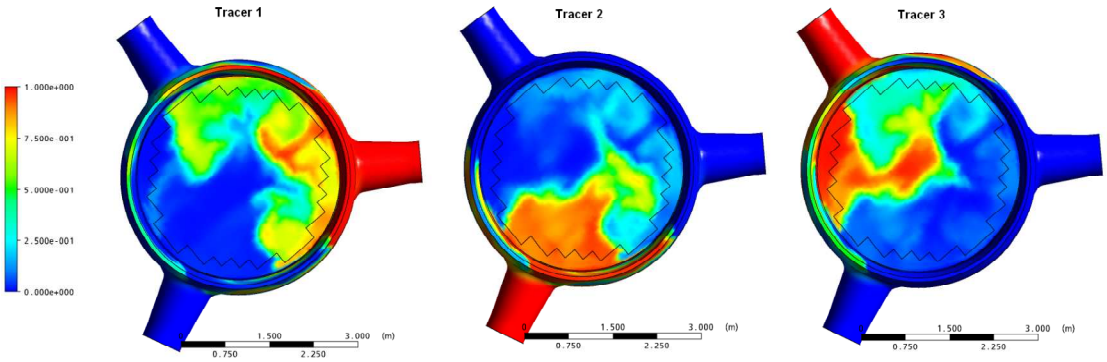

Figure 8 : Tracers distribution at the core inlet (case 1)

The geometry of the reactor pressure vessel has been analyzed in more details and it has been found that the different mixing behavior of the loops is mostly due to the holders for the core barrel and the thermal shields. When looking at the values given in Table 4 for the mixing coefficients, it is found that the mixing coefficient of loop 1 in the downcomer is well lower compared to the mixing coefficients in the downcomer of both other loops. From Figure 9 it can be seen that this is partly due to the holders for the core barrel. Indeed, this figure shows that both streams coming from loop 1 reach the location of a holder. Therefore, by going round this obstacle the flow coming from loop 1 gives a higher mixing. In contrary, it is seen that the streams coming from loop 2 barely reach the holder, and therefore loop 2 gives a lower mixing. The streamlines coming from loop 3 are not presented here, but the influences of the holder is somewhat higher than for loop 2, and as a result loop 3 gives an intermediate mixing. It is thought that the thermal shields in the downcomer also influence the mixing of the loops differently. More precisely, the thermal shields are thought to have an influence on the rotation of the flow. Indeed, the different intensity of the rotation between the loops might be due to the arrangement of the thermal shields around the downcomer that do not influence all loops in the same way. However, the effect of the thermal shields could not be analyzed in more details and therefore no conclusions should be taken so far.

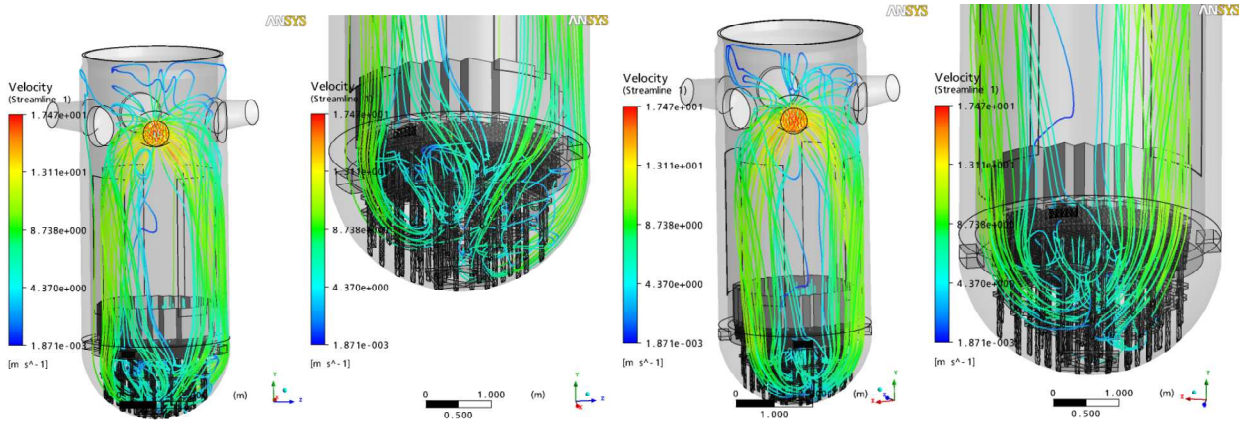

Figure 9 : Flow streamlines (case 1) coming from loop 1 (left) and from loop 2 (right)

4.3 Influence of the temperature on loop mixing coefficients

The aim of the second and third simulations is to analyze the influence of the temperature on the flow mixing of the loop with different temperature condition. With the same method as previously, the calculated loop 2 mixing coefficient amounts to 68.2 %, whereas for case 3 the loop 3 mixing coefficient is 63 %. When comparing those values to the one obtained for loop 2 and 3 in case 1 (same temperature in all three loops, see Table 4), it can be concluded that the mixing coefficient of the affected loop does not change much with the temperature. This conclusion can also be observed on Figure 10, when comparing it to Figure 8. Indeed, it is found that the tracer distribution of loop 2 and 3 at the core inlet does not change much compared to case 1. However, the mixing coefficients are global values, since the tracers mass flow is evaluated on a 120° sector. If the tracers distribution is analyzed locally at the scale of the fuel assemblies, the effect of temperature is more pronounced as it will be seen in the next section covering the flow distribution maps.

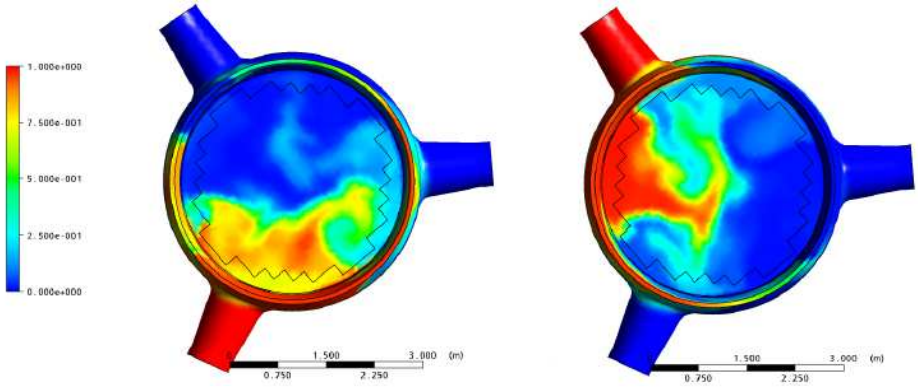

Figure 10 : Loop 2 tracer distribution at the core inlet for case 2 (left) and loop 3 tracer distribution at the core inlet for case 3 (right)

4.4 Flow distribution maps

The method used above for calculating the loop mixing coefficients can be generalized to derive flow distribution maps. More precisely, the mass flow of each tracer through each assembly has been calculated:

$$\dot{m}_{\phi_{i,j}} = \int_{A_j} \rho v \phi_i \tag{5}$$

where $\dot{m}_{\phi_{i,j}}$ is the mass flow of tracer i through assembly j and A_j is the flow section of assembly j. By dividing $\dot{m}_{\phi_{i,j}}$ by the total mass flow of assembly j, the ratio of the total assembly mass flow coming from the different loops is obtained:

$$x_{i,j} = \frac{\dot{m}_{\phi_{i,j}}}{\dot{m}_j} \tag{6}$$

where $x_{i,j}$ is the ratio of the total mass flow through assembly j coming from loop i and $\dot{m}_j$ is the total mass flow through assembly j. By following this method flow distribution maps can be produced that give the contribution of each loop to the assemblies' mass flow. Figure 11 gives the flow distribution map of loop 2 for case 1 and 2. As already explained in the previous section, the effect of the temperature on the flow mixing is more pronounced when considering those maps since they give a local evaluation of the flow mixing in contrast with the global evaluation given by the loop mixing coefficients. Based on the results of case 1, three maps have thus been derived (one for each loop). These are called the basic maps. It is observed that these basic maps are sensibly different depending on the loop to be considered. As explained before, this is due to the asymmetry of the reactor pressure vessel. Additional maps taking into account the effect of temperature have also been derived for loop 2 and 3. The coupled code package presented in section 2 can be improved by implementing these flow distribution maps, which give a more accurate modeling of the flow mixing. Indeed, the current PANTHER temperature distribution model considers flow distribution maps in six regions. The sensibility of the safety criteria to the new derived flow distribution maps for the asymmetrical transients will be assessed by sensitivity studies. This will be the next step of the present work.

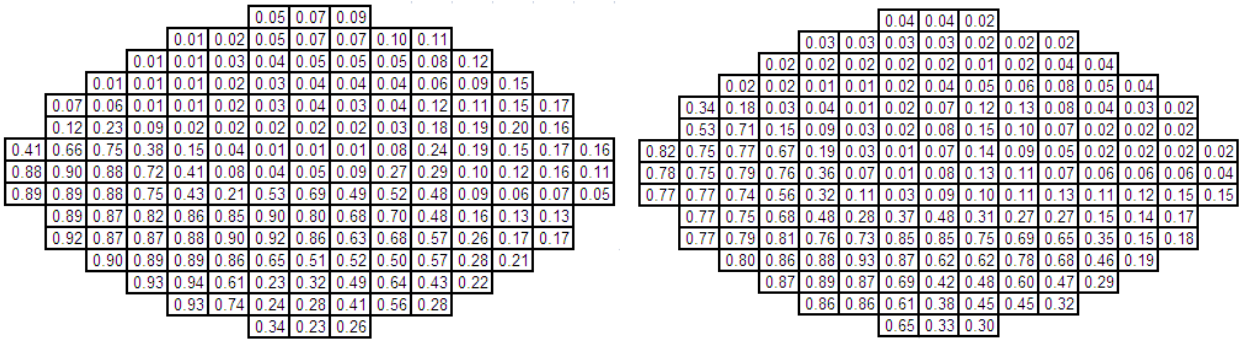

Figure 11: Flow distribution map of loop 2 for case 1 (left) and case 2 (right)

5. CONCLUSION

In the present study, CFD simulations have been used to assess the flow mixing in the reactor pressure vessel of Tihange 3. The realistic assessment of flow mixing is of particular importance for safety analysis, and more precisely for the evaluation of accidents leading to asymmetrical loop temperature conditions like for steam and feedwater line breaks. Before achieving the objectives, a benchmark of the CFD code has been performed. This validation step was necessary to demonstrate the potential of the CFD method to predict the relevant phenomena intervening in steady-state mixing conditions. To this end, CFD simulations of several steady-state mixing experiments conducted at the ROCOM facility were performed. The comparison of the CFD results with the experimental data has shown that the CFD results are qualitatively in good agreement with the experiments. Indeed, the relevant

physical phenomena observed in the experiments are also predicted in the CFD simulations. The asymmetrical velocity profile and the angular distribution of the flow in the downcomer were particularly in good agreement, as well as their variation with the loops flow rate asymmetry. At the core inlet the CFD results showed more differences with the experimental data. Indeed, it has been observed that the CFD simulations overestimate the mixing scalar at one side of the tracer sector. Further sensitivity studies should be performed on hexahedral meshing, which might decrease numerical diffusion and give insight on the disagreements observed at the core inlet.

For the simulations of the flow mixing in the Tihange 3 pressure vessel, the results have shown that the mixing assumptions used in the current safety analyses are conservative. Indeed, the RELAP5 mixing coefficients implemented in the current model are well higher (85 %) compared to the mixing coefficients calculated with the CFD method (less than 65 %). The analysis has also shown that the mixing behavior is not equivalent between the different loops, due to the asymmetry of the reactor pressure vessel. This effect has been investigated in more details and the difference is thought to come from the upper part of the vessel, and more precisely from the holders for the core barrel and the thermal shields. The effect of temperature on the flow mixing of the loop with different temperature condition has been analyzed and it has been shown that this effect is negligible on the loop mixing coefficient. However, the influence of the temperature can be important locally as it has been shown on the flow distribution maps. With their implementation in the coupled code package, the results of the CFD simulations have the potential to improve the current safety analyses. Indeed, the consideration of these results would yield a more realistic assessment of the transients behavior.

REFERENCES

[1] T. Höhne, “Modeling of a Buoyancy-Driven Flow experiment in Pressurized Water Reactors using CFD-Methods”, *Nuclear Engineering and Technology,* vol. 39, 327-336 (2007)

[2] T. Höhne, “Numerical simulation of coolant mixing in a pressurized water reactor with different CFD methods based on complex meshes”, *International Journal of Nuclear Energy Science and Technology,* vol. 3, 399-412 (2007)

[3] S. Kliem, “Experiments on slug mixing under natural circulation conditions at the ROCOM test facility using high-resolution measurement techniques and numerical modeling”, *Nuclear Engineering and Design,* (2009)

[4] H.-M. Prasser, “Coolant mixing in a PWR - deboration transients, steam line breaks and emergency core cooling injection - experiments and analyses”, *Nuclear Technology,* vol. 143, 37-56 (2003)

[5] U. Rohde, “Application of CFD codes in nuclear reactor safety analyses”, *Science and Technology of Nuclear Installations,* (2009)

[6] U. Rohde, “Fluid mixing and flow distribution in a primary circuit of a nuclear pressurized water reactor - Validation of CFD codes”, *Nuclear Engineering and Design,* vol. 237, 1639–1655 (2007)

[7] U. Rohde, “Fluid mixing and flow distribution in the reactor circuit, measurement data base”, *Nuclear Engineering and Design,* vol. 235, 421-443 (2005)

[8] U. Rohde, “The European project FLOMIX-R : Fluid mixing and flow distribution in the reactor circuit, Final Summary Report”, Report FZR 432, Rossendorf, Dresden, Germany (2005)

[9] T. Toppila, “The European project FLOMIX-R : description of the experimental and numerical studies of flow distribution in the reactor primary circuit (Final report on WP 3)”, FLOMIX-R-D10, Fortum Nuclear Services, Espoo (Finland), 2004